Lattice Boltzmann simulations of sedimentation of a single fiber in a weak vertical shear flow

Dewei Qi, Guowei He, and Yingming Liu

Citation: Physics of Fluids (1994-present) **25**, 093302 (2013); doi: 10.1063/1.4821775
View online: http://dx.doi.org/10.1063/1.4821775
View Table of Contents: http://scitation.aip.org/content/aip/journal/pof2/25/9?ver=pdfcov
Published by the AIP Publishing

PHYSICS OF FLUIDS **25**, 093302 (2013)

Lattice Boltzmann simulations of sedimentation of a single fiber in a weak vertical shear flow

Dewei Qi,[1] Guowei He,[2] and Yingming Liu[3]
[1]*Department of Chemical and Paper Engineering, Western Michigan University, Kalamazoo, Michigan 49009, USA*
[2]*Stake Key Laboratory of Nonlinear Mechanics, Institute of Mechanics, Chinese Academy of Sciences, Beijing 100080, People's Republic of China*
[3]*Yangtze Center of Mathematics, Sichuan University, Chengdu 610064, China*

(Received 3 April 2013; accepted 24 August 2013; published online 23 September 2013)

Instability of a suspension is directly related to the problem of the cross-stream migration of a particle relative to its neighboring particle suspension. Such cross-stream or lateral migration of a single non-spherical particle (fiber) settling in a bounded weak shear flow with vertical streamlines produced by a perturbation to the fiber number density is studied using lattice Boltzmann simulations. The present simulation results demonstrate that at a given shear rate, the lateral migration can be divided into three phases depending on settling Reynolds number R_{sd} and particle aspect ratio κ. At a low settling Reynolds number R_{sd}, the suspension becomes more stable in phase 1. As R_{sd} increases and excesses a critical settling Reynolds number R_{sd1}, the fiber suspension becomes unstable in phase 2. In phase 3, at an enough large R_{sd}, the inertia dominates the weak shear flow and it may have little effect on stability. A mechanism of the instability induced by an inertial fiber orientation drift and a shear induced cross-streamline drift, recently proposed by Shin, Koch, and Subramanian ["Structure and dynamics of dilute suspensions of finite reynolds number settling fibers," Phys. Fluids **21**, 123304 (2009)], is examined and confirmed.
 [http://dx.doi.org/10.1063/1.4821775]

I. INTRODUCTION

Sedimentation is popularly used to separate solid particles from fluids or classify the different particles in term of their sizes by chemical engineers. For instance, in the paper industry, fines can be separated from long fibers by a sedimenting process since fines have huge surface areas, receive larger drag, and settle slowly. When fibers in suspensions settle down vertically due to gravity, a weak vertical shear flow may be created within the suspension due to the variation of fiber number density. A fiber within the suspension may experience a shear force and migrate laterally either toward the downward flowing fluid region with the high particle number density or toward the lower particle number density region depending on the settling Reynolds numbers $R_{sd} = V_z l/\nu$, where V_z is the terminal settling velocity of the mass center of the fiber in the gravity direction or z-direction; l is the half fiber length; and ν is the kinematic viscosity.

In the Stokes flow regime, Koch and Shaqfeh[1] recognized that motion of a fiber due to gravity depends on its orientation. The settling velocity is twice as large when it settles with its long body vertically as when it does with its long body horizontally. The anisotropic resistance to a translation motion leads to a horizontal migration. When two fibers are randomly oriented, the two fibers will settle with different velocities, one faster than other. When one fiber settles through the region surrounding the second fiber, both the fiber orientations will be changed. Through computing the probability of finding one fiber near other fiber, they predicted that the long range hydrodynamic interaction between the two fibers will drive one fiber to laterally drift to the other fiber. They further evidenced that a variation of fiber number density in the horizontal direction will induce a weak vertical shear flow field and under its influence the fiber will laterally migrate toward the downward

flowing fluid region with a higher fiber number density. Thus, the fiber suspension becomes more inhomogeneous and unstable. Unlike fibers, spherical particles will migrate in the opposite direction and are spatially distributed more homogeneous under the same condition due to its symmetrical property in all directions.

This important problem including nonzero Reynolds numbers[2,3] has been investigated by many authors and recently reviewed by Guazzelli and Hinch.[4] Experiments and numerical simulations[5–10] confirmed the findings of Koch and Shaqfeh and showed that in a dilute suspension the fibers tend to coagulate and the mean settling velocity of a fiber cluster may be larger than that of an isolated single fiber aligned with its long body vertically when R_{sd} is small enough. When the Reynolds number is nonzero, the force and torque on a settling fiber have been computed using a slender-body theory in the limit of small Reynolds number by Khayat and Cox[11] and at finite Reynolds number by Shin *et al.*[12] To understand how the lateral migration of a settling fiber responds to the vertical shear flow produced by a perturbation to the fiber concentration at a finite Reynolds number, Shin *et al.*[13] conducted a linear stability analysis by using the slender-body theory coupled with a pseudospectral solution of the Navier-Stokes equation. They proposed that there are two factors which control the lateral migration of a finite Reynolds number fiber in a vertical shear flow. The first factor is called "shear induced drift" associated with fluid and solid particle translational and rotational inertia. A vertical shear fluid flow with stream lines downward is imposed as shown in Figure 1. The shear flow can be expressed by $U_z(y) = Gye_z$, where U_z is the undisturbed fluid velocity in the vertical or z-direction; G is the shear rate; e_z is the unity vector of the z-axis; and x,y,z are the coordinate variable in the vorticity, shear gradient, and gravity direction, respectively. When the fiber in Figure 1 is replaced by a spherical solid particle (not shown) with a density of $\rho_s > 1.0$ (where the particle density is normalized by the fluid density and this definition is applied throughout this work), the settling velocity is larger than the local fluid velocity. A lift due to inertia drives the particle to migrate in the negative y-direction with a velocity $V_y < 0$. When the solid particle density is less than 1, the settling velocity lags the local fluid velocity and the particle migrates in the opposite direction. This was originally found by Saffman[14] in the limit of the weak inertia $R_{sd} \ll R_s^{(1/2)} \ll 1$, where the shear Reynolds number is defined by $R_s = Gl^2/\nu$. Later, other authors' theoretical work and simulation results[15,16] show that the Saffman mechanism is valid at a large particle settling Reynolds number up to 50.[17–19] The Saffman mechanisms initially found for spherical particle persists for a nonspherical particle system.

The second factor is called "orientation drift." A fiber at finite Reynolds number attempts to align its long axis with the horizontal direction due to nonlinear inertial torque. This tendency increases as R_{sd} increases. On the other hand, the torque due to the imposed vertical weak shear rotates the fiber in the opposite direction if the fiber is oriented as shown in Figure 1. The balance between the two torques results in an inclined angle between the fiber axis and the horizontal direction within the extensional quadrant of the shear flow and drives the fiber to migrate toward the streamlines with the larger downward flow velocity. The second factor only exists in a nonspherical particle. Certainly, the combination of the two factors will determine the final net cross-stream or lateral migration and in turn determine the stability of suspensions at finite Reynolds number.

Regarding the shear induced drift for a slender fiber, based on the slender body theory in the limit of $S = \frac{R_s}{R_{sd}} \ll 1$ and $R_{sd} \sim O(1)$, Shin *et al.*[13] expended the fiber orientation vector to the first order of the orientation perturbation in parameter S due to the small shear velocity disturbance and found that the shear induced drift always reinforces the orientation drift for all R_{sd}

Subsequently, they conducted numerical simulations of sedimentation of many fibers and the results of mean settling velocity, fiber orientation distribution, structure factors, fiber and fluid velocity fluctuation confirmed that the fiber suspension is unstable and the fibers do turn their long body along the horizontal direction at a dilute concentration as the Reynolds number increases although this horizontal alignment probability decreases as the fiber concentration increases. In their simulation, the slender body approximation without including the fiber volume effect was used and a large aspect ratio $\kappa = 10$ is adopted. Their results are comparable with the results of Kuusela *et al.*[20,21] who used immerse boundary method in which the fluid is allowed to enter the solid particle.

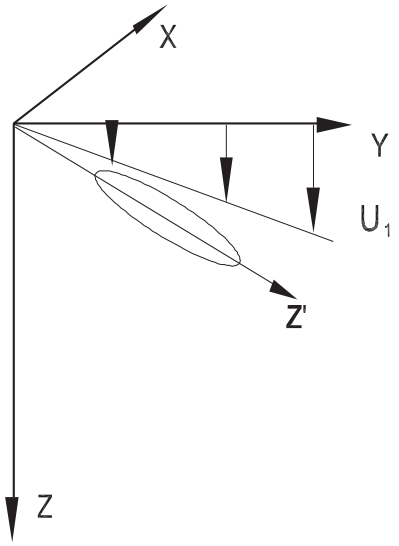

FIG. 1. A shear velocity field $U_z(y) = Gye_z$ is imposed along the y-axis, the vorticity of the weak shear is in the x-direction, and the gravity is in the z-direction. θ (not shown) is the polar angle between the fiber z′-axis and z-axis and the ϕ (not shown) is the angle between the y-axis and the projection of the fiber z′-axis on the xy-plane.

The present work conducts a series of numerical simulations of a single sedimenting fiber in a bounded weak vertical shear flow by using the lattice Boltzmann method. The mechanism proposed by Shin *et al.* is numerically examined once again in the same range of Reynolds number $R_s \ll R_{sd} \sim O(1)$ as they used and the influence of the imposed weak vertical shear flow on lateral migration at different values of R_{sd} and κ will be investigated. We are particularly interested in a low aspect ratio around $\kappa \sim O(1)$ and want to see if the mechanism proposed by Shin *et al.* in the high aspect ratio is valid for a low aspect ratio. In addition, as mentioned before, the shear-induced drift is in the negative y-direction for a spherical particle and one would probably expect that there is a critical low aspect ratio for a nonspherical particle to reverse the shear induced drift direction at a finite R_{sd} according to Shin *et al.* Therefore, three levels of $\kappa = 1.2$, 1.6, and 2 are used in the present simulation.

We make a remark here. The present results are obtained from $R_{sd} \sim O(1)$ and a net cross-streamline migration signals either a stable or unstable suspension depending on the sign of the migration velocity. Unlike the case of $R_{sd} \sim O(1)$, a single fiber at $R_{sd} = 0$ will rotate in Jeffrey obits,[22] oscillate in the y-direction, and have a no net drift in the horizontal direction at all although the fiber system is unstable. Therefore, the mechanism of Shin, Koch, and Subramanian[13] is intrinsically different from the mechanism of Koch and Shaqfeh.[1] It is pointed out that the instability mechanism of Koch and Shaqfeh[1] still holds at small but non-zero Reynolds number, but at modified growth rates, as shown by Dahlkild[2] and by Zhang *et al.*[3]

Section II presents the simulation conditions; Sec. III will report the simulation results of the cross-steam migration at different R_{sd}, R_s, and aspect ratio. It is found that the migration can be classified into three different phases. The lateral migration phase separation diagram is drawn. Section IV gives some conclusion.

II. SIMULATION PARAMETERS

A vertical shear fluid flow is initially set with velocity $U_z(0) = 0$ at the left wall and with velocity $U_z(N_y) = U_1$ at the right wall, as shown in Figure 1. A prolate spheroidal fiber with a half length of $l = 0.5L$ is used, where L is the fiber length, and its aspect ratio may be varied at $\kappa = 2$, 1.6, and 1.2 in the simulations. Simulations are carried out in a box of $64 \times 64 \times 128$ where the confinement ratio is $C = L/N_y = 0.375$. The effect of the confinement ratio is not a current focus and will not be investigated in the present work. All the fibers are initially located at the center

between the two walls $Y/N_y = 0.5$ with their principal z'-axis parallel to the horizontal direction. The different settling Reynolds numbers R_{sd} are obtained by varying solid density ρ_s and kinematic viscosity ν while the time and length units are kept same. A periodic boundary condition is imposed in the vertical direction during simulation. The lateral or crossing stream migration and rotation are allowed. In a short time period the fiber will migrate in the y-direction and rotate around its short axis only that is parallel to the x-axis. This rotation is limited on the vertical yz-plane. The rotational polar angle θ between the fiber principal z'-axis and the vertical direction or z-axis can be defined. Most simulations in the present work are limited to the short period time. However, after a long time period, the fiber may also migrate in the x-direction and rotate around the z-axis about ϕ defined by the angle between the project of the fiber z′-axis on the xy-plane and the y-axis. This angle ϕ is on the xy-plane. We will come back to this point later.

A lattice Boltzmann method with 3DQ15 model is adopted.[23] The method has been reported[24–29] previously and will not be repeated here. The length is normalized by the tunnel width N_y and the velocity is normalized by $U_0 = 10N_yG$ for this report where the shear rate $G = \frac{U_1}{N_y} = 0.000111$. All variables are nondimensionalized in the simulations.

III. SIMULATION RESULTS

A. Phase transition of lateral migration

It is found that at a given shear Reynolds number R_s, fiber lateral migration can be divided into three different phases depending on the settling Reynolds number R_{sd} and fiber aspect ratio κ.

At a low settling Reynolds number, nonlinear inertial effects are very weak and the imposed vertical shear may dominate the inertia. The shear force drives the fiber to rotate and tumble periodically with an angular amplitude $\theta = 180$ (see Figure 3(b)). The fiber migrates in the negative y-direction with a steady oscillation as shown in Figure 2 for its lateral migration and velocity and in Figure 3 for its vertical velocity and fiber orientational angle θ in the case of $R_s = 0.1$ and $\kappa = 1.6$. On a time average, a net migration in the horizontal direction results in $Y/N_y < 0.5$.

The relative velocity of the fluid flow to the fiber in its left is larger than that in the right and the generated pressure difference between the two sides forces the fiber to migrate in the negative y-direction with $V_y < 0$. Finally the lateral migration is stopped, on time average, near the left wall until the lift force is balanced by the wall repulsion. This type of force balance is similar to Segré and Silberbergi phenomena[30,31] where the settling velocity leads the local fluid velocity.[32] This is called phase 1. It seems that the lateral migration in the negative y-direction increases as R_{sd} decreases in phase 1. This is true only when $R_{sd} \sim 1$. The probability of the fiber alignment with the horizontal direction decreases as R_{sd} decreases. The weak shear plays a major role. As we mentioned before, when $R_s \ll R_{sd} \ll 1$, say $R_{sd} \sim 10^{-4}$, the fiber rotates in the Jeffrey orbits and have a no net migration since inertia is entirely neglected. We do not include the cases of $R_{sd} < 0.1$ in this paper.

As R_{sd} increases and becomes larger than a critical value $R_{sd} > R_{sd1}$, the inertia becomes large enough and the fiber tends to be aligned with the horizontal direction. The inertial alignment may be balanced by the imposed weak shear, a small angle between the horizontal direction and fiber axis is created. The fiber will migrate along the inclination angle, with respect to the horizontal direction, with $V_y > 0$ until it is stopped in the lateral direction by a wall repel force. The results are shown in Figure 4(a) for its lateral displacement, Figure 4(b) for lateral velocity, Figure 4(c) for settling velocity, and Figure 4(d) for orientational angle. In other words, as the fiber moves to higher concentration regions, inhomogeneities in spatial fiber distribution are enhanced. This is phase 2.

It is found that there are three different cases in phase 2. First, at a lower settling Reynolds number, for instance, $R_{sd} = 1.028$, the fiber always dynamically rotates with an angular amplitude of $\theta = 180^\circ$ and constantly oscillates in the y-direction, as shown in Figure 4(a) for the migration and Figure 4(d) for the rotational angle. Although the fiber never has a fixed orientation, on time average it spends more time, due to orientational inertia, statistically in the direction for which $V_z > 0$ than in the direction for which $V_z < 0$. The final average cross-stream position Y/N_y is slightly larger than 0.5. Second, as the settling Reynolds number increases, the fiber position and orientation initially oscillates and finally becomes stable such as in the case of $R_{sd} = 1.203$. This oscillation case is

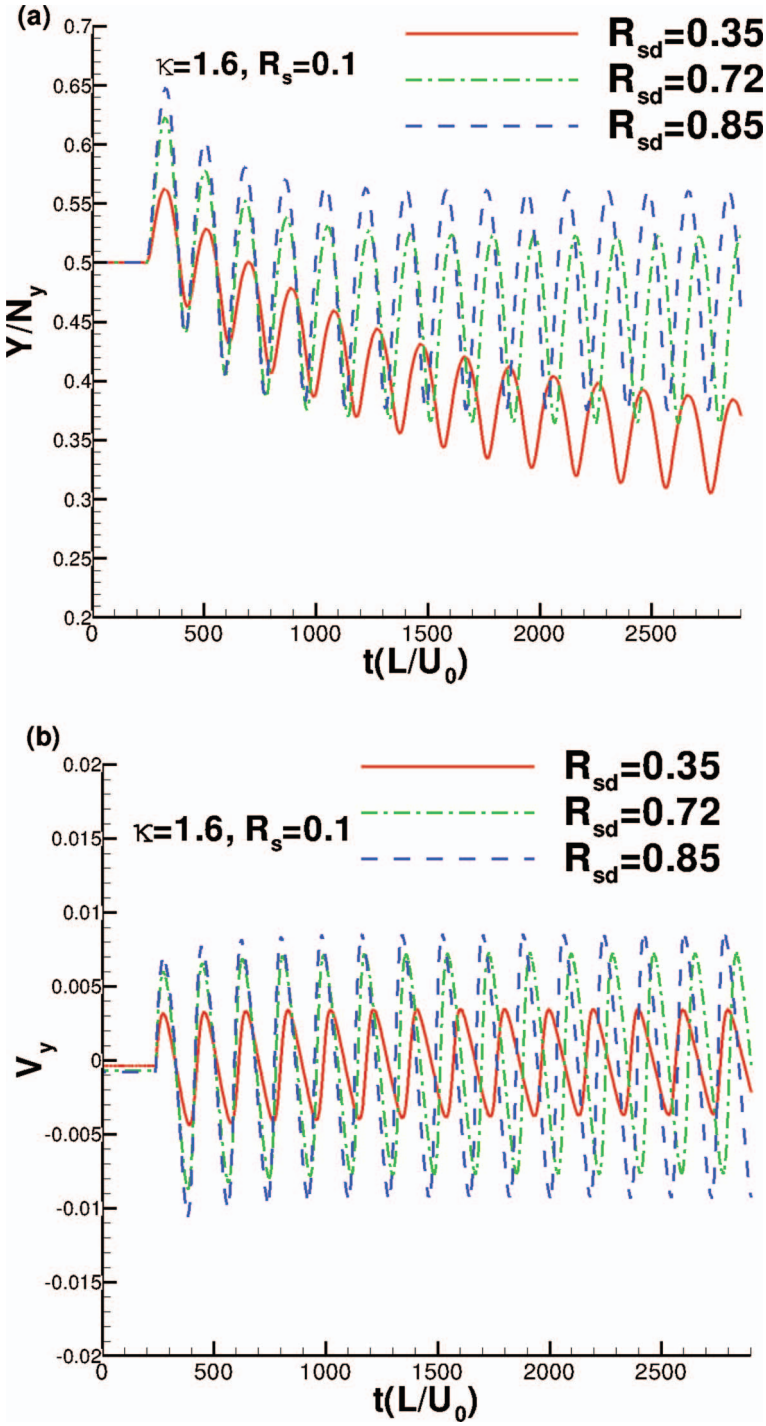

FIG. 2. (a) Lateral migration displacement and (b) lateral velocity of fiber as a function of time at different settling Reynolds numbers in the phase 1 for the case of $R_s = 0.1$ and $\kappa = 1.6$.

consistent with the observation of Huang *et al.*[33] In the third case, the lateral migrations of the fiber at $R_{sd} = 1.74$, 2.35, and 3.51 have no oscillation. In general, it is shown that the lateral migration reduces as R_{sd} increases due to the angle gradually approaching to 90°.

As R_{sd} increases continuously until it is larger than a 2nd critical number $R_{sd} > R_{sd2}$ the fiber inertial alignment may dominate the weak shear and maintain its long axis horizontally. Thus, the

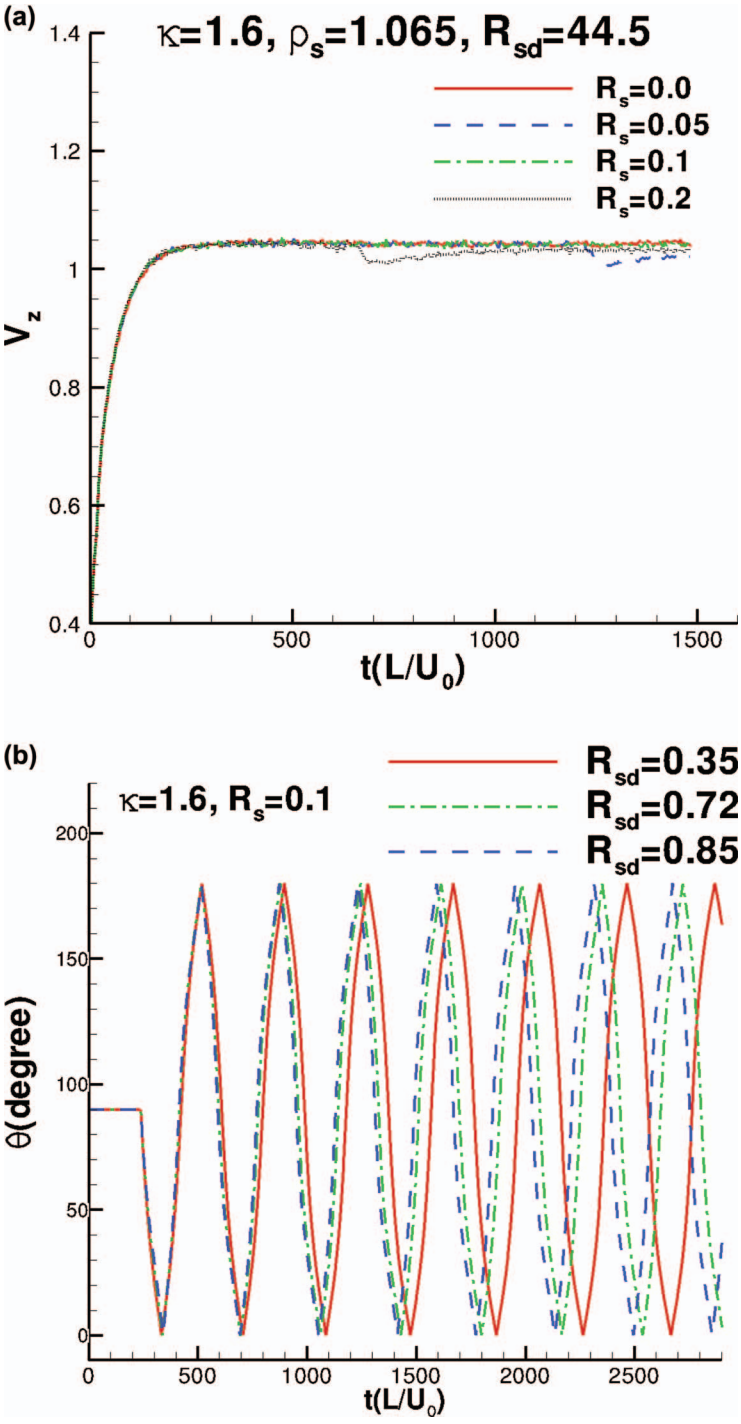

FIG. 3. (a) The fiber vertical velocity and (b) orientational angle θ as a function of time at different settling Reynolds numbers in the phase 1 for the case of $R_s = 0.1$ and $\kappa = 1.6$.

fiber may remain in the center between the two walls. This is phase 3. At a large settling Reynolds number, although the wake effect may induce oscillation of both orientational angle and lateral migration around their corresponding equilibrium position, the lateral migration diminishes on average of time. As shown in Figure 5 for the lateral migration and velocity, the vertical velocity and orientational angle, when R_{sd} increases from 24.02 to 44.51, although the amplitude of oscillation

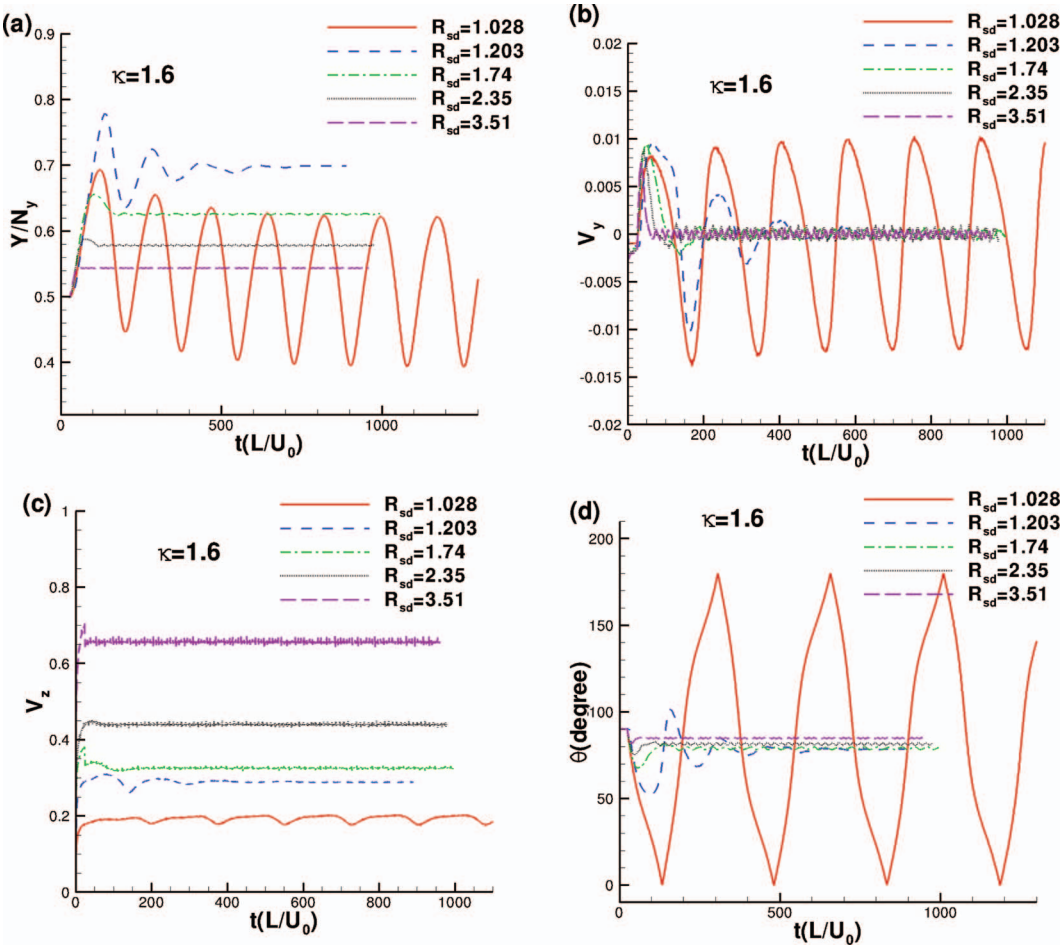

FIG. 4. (a) Lateral migration displacement, (b) lateral velocity, (c) vertical velocity, and (d) orientation angle as a function of time at different settling Reynolds numbers R_{sd} in the phase 2 for the cases of $\kappa = 1.6$.

of both the lateral displacement and orientation angle increases, the average lateral migration does not change too much, indicating that the lateral migration in phase 3 is clearly independent of R_{sd}. The oscillation is caused by the wake effect or vortex behind the fiber. For the case of $R_{sd} = 44.51$, the Strouhal number is around 0.026. It is noted that the vortex shedding does not affect the lateral migration.

Further, it is obvious that the lateral migration will be influenced by the aspect ratio. Numerous simulations are conducted at $\kappa = 1.2$, 1.6, and 2 for the case of $R_s = 0.1$ and at $\kappa = 1.6$ and 2 for the cases of $R_s = 0.05$ and 0.2, respectively, to illustrate the corresponding phase transitions. The migration results are collected and expressed in a coordination system of R_{sd} against aspect ratio κ as a phase diagram shown in Figure 6. We make a remark here. The current work has no intention to accurately identify the phase diagram. It is not possible for one to accurately obtain the phase diagram by using numerical simulation results because numerical fluctuation brings an error for determination of the final position of the lateral migration.

At a given shear Reynolds number, as κ decreases, the first critical settling Reynolds number increases. This is what one expects because the fiber with a smaller aspect ratio needs to have a larger settling Reynolds number to balance the given shear force. In contrary, as κ decreases, the second critical settling Reynolds number decreases, because the fiber with a smaller κ is easier to migrate with $V_y < 0$ and therefore has a lower second critical settling Reynolds number.

It is noted that the analysis of Shin *et al.* is based on a simple shear without walls and a very large aspect ratio is used in their analysis while two walls are included and a low aspect ratio $O(1)$ is

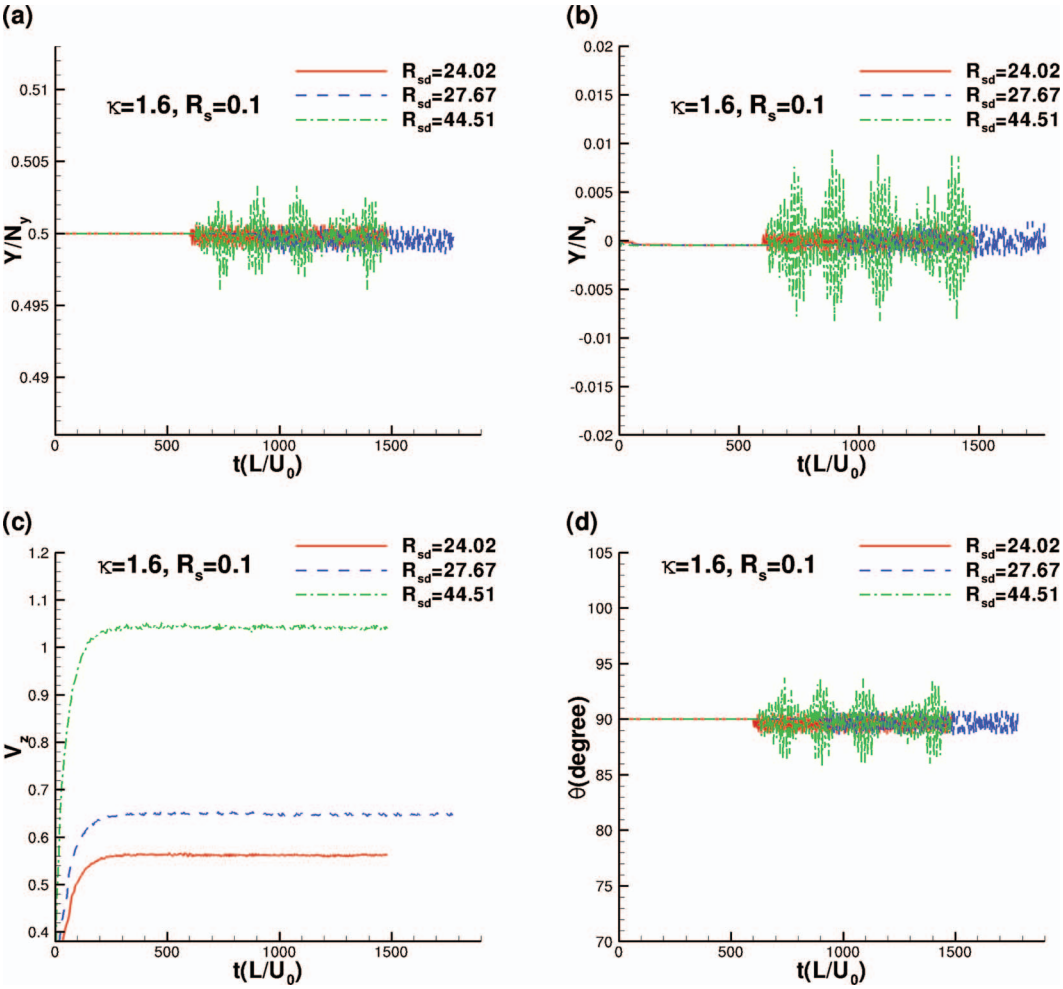

FIG. 5. (a) Lateral migration displacement, (b) lateral velocity of fiber (c) vertical velocity, and (d) orientational angle as a function of time at different settling Reynolds numbers for the case of $\kappa = 1.6$ in phase 3.

used in this work. The different wall boundary condition and aspect ratio may lead to a difference. The results of the fiber laterally migrating with $V_y > 0$ in phase 2 are consistent with their analysis results while the results of the fiber migrating to the lower concentration region with $V_y < 0$ in phase 1 may be caused by the wall effect and limited by the small aspect ratio.

B. Effects of shear rate

At a given R_{sd}, effect of the shear Reynolds R_s on migration is different in the three phases. In phase 1, at $R_{sd} = 0.7$, as the shear Reynolds number increases from $R_s = 0.1$ to 0.2, the fiber migration with $V_y < 0$ increases as shown in Figure 7 due to an increasing pressure difference on the left and right sides of the fiber. In phase 2, when $R_{sd} = 2.4$, as the shear Reynolds number increases from $R_s = 0.05$ to 0.1 and 0.2 the fiber inclination angle with respect to the horizontal axis increases, resulting in a larger migration with $V_y > 0$ as shown in Figure 8(a) for the lateral migration and Figure 8(b) for the orientational angle in the case of $\rho_s = 1.2$ and $\kappa = 1.6$. However, if the shear rate is too large and excesses a critical value, then the shear force overcomes inertial torques, rotates fiber continuously, and reduces the lateral migration. When $R_s = 0.3$, the fiber is tumbling and rotating, the lateral migration is largely reduced as shown in Figure 8(c) and the angle varies between 0° and 180° as shown in Figure 8(d).

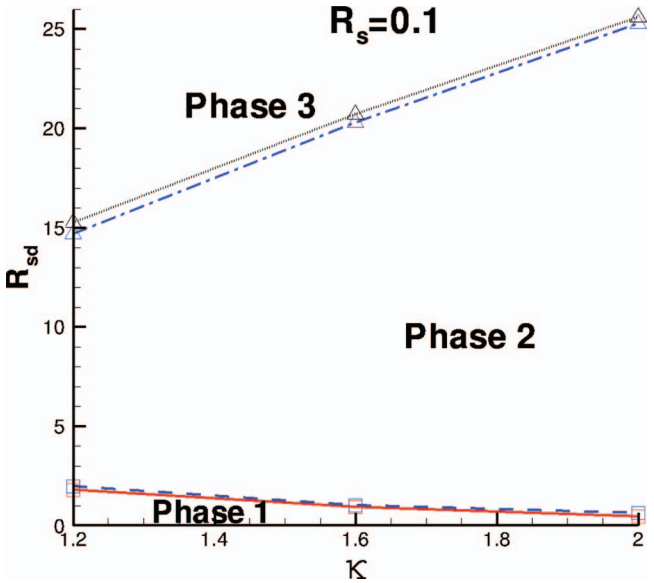

FIG. 6. At a given shear Reynolds number $R_s = 0.1$, the fiber lateral migration can be divided into three phases in a coordination system of R_{sd} against aspect ratio κ. The critical transition of settling Reynolds number from phase 1 to 2 may be located between the lines with squares and that from phase 2 to 3 may be located between the lines with triangles.

In phase 3, since the inertia dominates the weak shear, the shear Reynolds number R_s has little effect on the lateral migration at a given $R_{sd} = 44.5$. When shear Reynolds number R_s increases from 0.0 to 0.1 and 0.2 while the particle density and aspect ratio are kept at $\rho_s = 1.065$ and $\kappa = 1.6$, the lateral migration does not change too much as shown in Figure 9. It is shown that at the Reynolds number of $R_{sd} = 44.5$ the lateral migration is insensitive to or independent of the shear rate.

C. Long time migration

As described before, the inertial torques due to sedimentation may rotate the fiber around the x-axis and align its long axis with the horizontal direction. On the other hand, the imposed weak shear flow will tend to rotate fiber to align with the vertical direction. The time required to establish an equilibrium balance between the two torques for $R_{sd} = O(1)$ is about L/V_y. For the case of $R_{sd} > R_{sd1}$, in a short time period, the fiber lies and rotates on the zy-plane and migrates in the region of phase 2. However, over much longer time period $O(L/V_y R_s^{-1})$, inertia may cause the fiber to rotate around z-axis with an angle of ϕ, and finally turn the fiber long axis along the vorticity direction. Thus, the symmetrical circular cross-section of the fiber is on the yz-plane and seen by the weak shear flow. Therefore, the fiber will finally migrate in the region of phase 1 similar to the case of a spherical particle. A simulation of a fiber with the aspect ratio of $\kappa = 2$ is conducted at $R_s = 0.1$ for a long time period run. Figure 10(a) shows that the fiber migration transfers from one state, where the fiber long axis lies on the yz-plane and the fiber migrates in the region of phase 2 due to fiber anisotropy in short time period, to another state, where the fiber long axis is perpendicular to the yz-plane and the fiber migrates in the region of phase 1 due to the circular cross section seen by the shear field after a long time period. The former corresponds to the state of $R_{sd} = 1.68$ for a short time period and the later corresponds to the state of $R_{sd} = 0.89$ for a long time period in Figure 10. Figures 10(b) and 10(c) show that the fiber with $\theta = 83^\circ$ and $\phi = 0^\circ$ initially migrates in phase 2. After a long time period, the fiber also rotates about the z-axis and finally has an orientation with $\phi = 90^\circ$ and $\theta = 90^\circ$ as shown in Figures 10(b) and 10(c). Thus, the fiber long axis is parallel to the vorticity and migrates in phase 1.

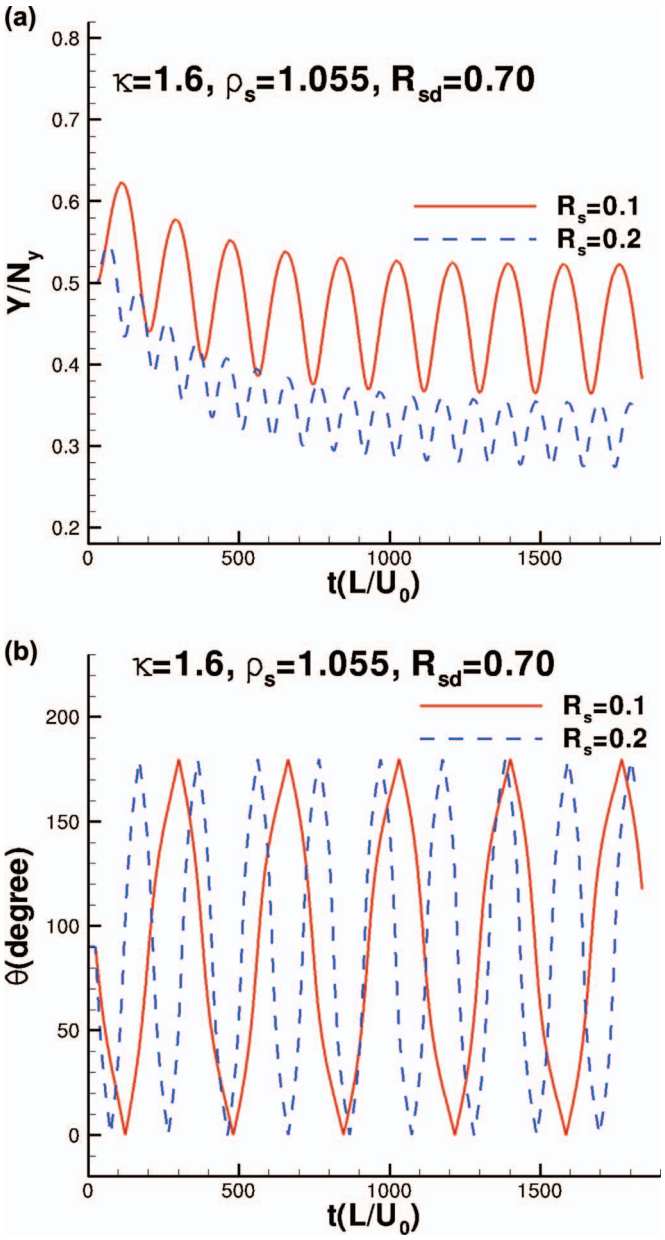

FIG. 7. (a) The fiber lateral migration and (b) orientational angle θ at $R_s = 0.1$ is compared with those at $R_s = 0.2$ in phase 1 (the fiber density and fluid viscosity are the same).

IV. DISCUSSION AND CONCLUSIONS

Based on the prediction of the analysis of Shin *et al.*,[13] hundreds of lattice Boltzmann simulations are conducted to investigate the effects of interaction between hydrodynamics and settling non-spherical particles on the stability of suspensions. In the simulations, a single prolate spheroidal fiber is settling in a vertically bounded linear weak shear field. The fiber receives a lift force and migrates laterally. Since the imposed shear field represents the influence of motion of other neighboring fibers in suspensions and is driven by horizontal inhomogeneities in the fiber concentration, the direction of the cross-stream or lateral migration is directly related to the stability of the suspension at $R_{sd} \sim O(1)$. The simulation results demonstrate that at a given shear rate and a given particle aspect ratio, the cross-stream or lateral migration can be divided into three phases. At a low settling

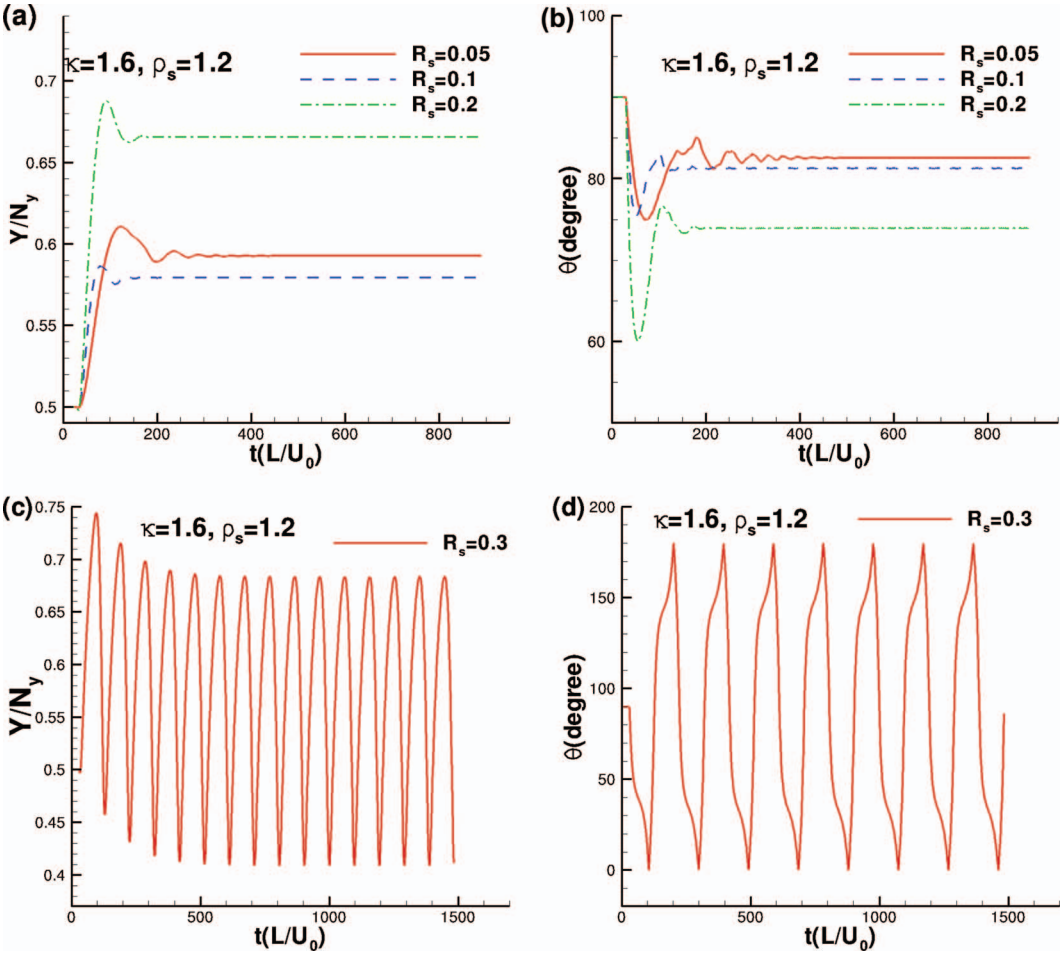

FIG. 8. (a) The fiber lateral migration and (b) orientational angle θ are compared among the cases with different $R_s = 0.05$, 0.1, and 0.2; (c) the fiber lateral migration for the case of $R_s = 0.3$ and (d) orientational angle θ for the case of $R_s = 0.3$ while the fiber density $\rho_s = 1.2$, $\kappa = 1.6$, and other conditions are the same for all the cases. The settling Reynolds number is about 2.4.

Reynolds number, the shear force may dominate the inertia and the fiber may tumble and migrate with $V_y < 0$. This is phase 1 where the fiber suspension becomes more homogeneous and stable. As the Reynolds number R_{sd} increases and excesses a critical Reynolds number R_{sd1}, the fiber attempts to align its long axis with the horizontal direction due to the inertial torque. This torque may be balanced by the imposed shear force, resulting in an inclined angle between the fiber axis and the horizontal plane and driving a lateral migration toward the denser fiber particle region ($V_y > 0$). This is phase 2 where the inhomogeneity is reinforced. As the settling Reynolds number continuously increases and excesses the second critical number R_{sd2} such that the inertia dominates the weak shear force, the fiber long axis is kept in the horizontal direction and may remain in the center between two walls. This is phase 3 where the fiber has little lateral migration and it is independent of Reynolds number. It is demonstrated that in phase 1 the lateral migration with $V_y < 0$ increases as the shear rate increases while in phase 2 the lateral migration with $V_y > 0$ reduces as the Reynolds number increases. In phase 3, the inertia dominates and the shear rate has little effect on lateral migration. A lateral migration phase diagram can be obtained by plotting R_{sd} as a function of particle aspect ratio. The mechanism of the instability induced by a shear induced cross-streamline drift and an inertial fiber orientation drift, recently proposed by Shin, Koch, and Subramanian,[13] is confirmed.

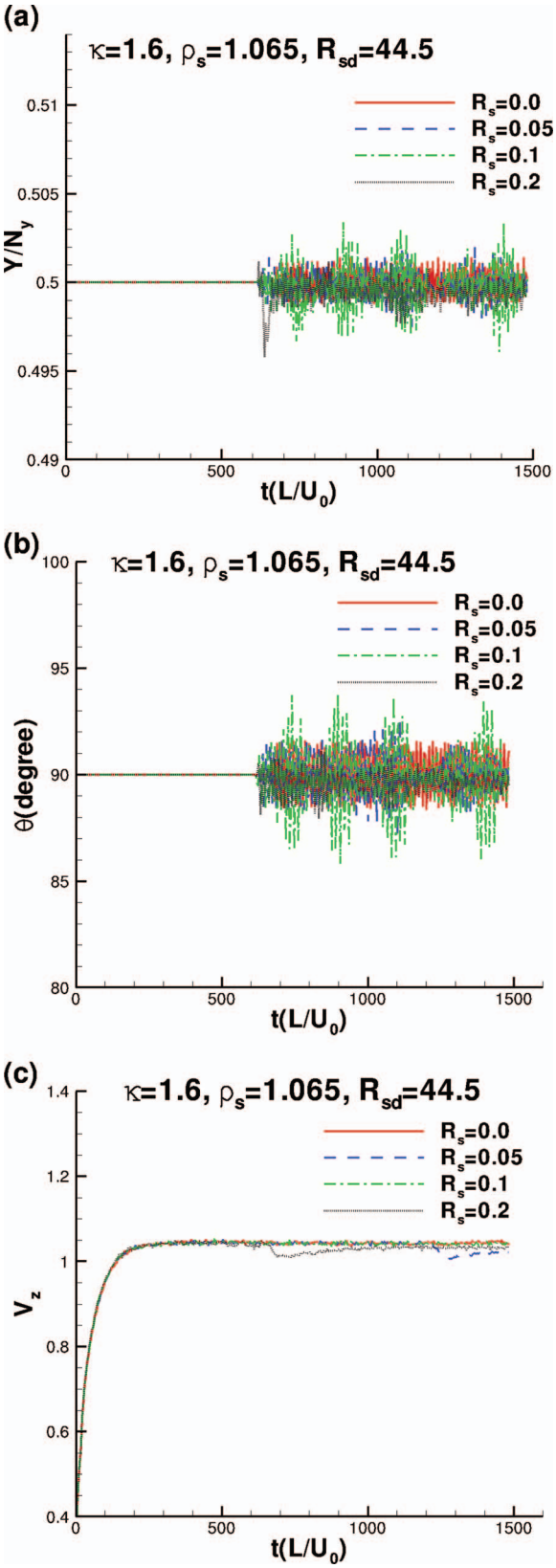

FIG. 9. (a) The fiber lateral migration, (b) orientational angle θ, and (c) vertical settling velocity at $R_s = 0.0$, 0.05, 0.1, and 0.2, respectively, for the case of $\rho_s = 1.065$ and $\kappa = 1.6$ are compared. The settling Reynolds number is about 44.5.

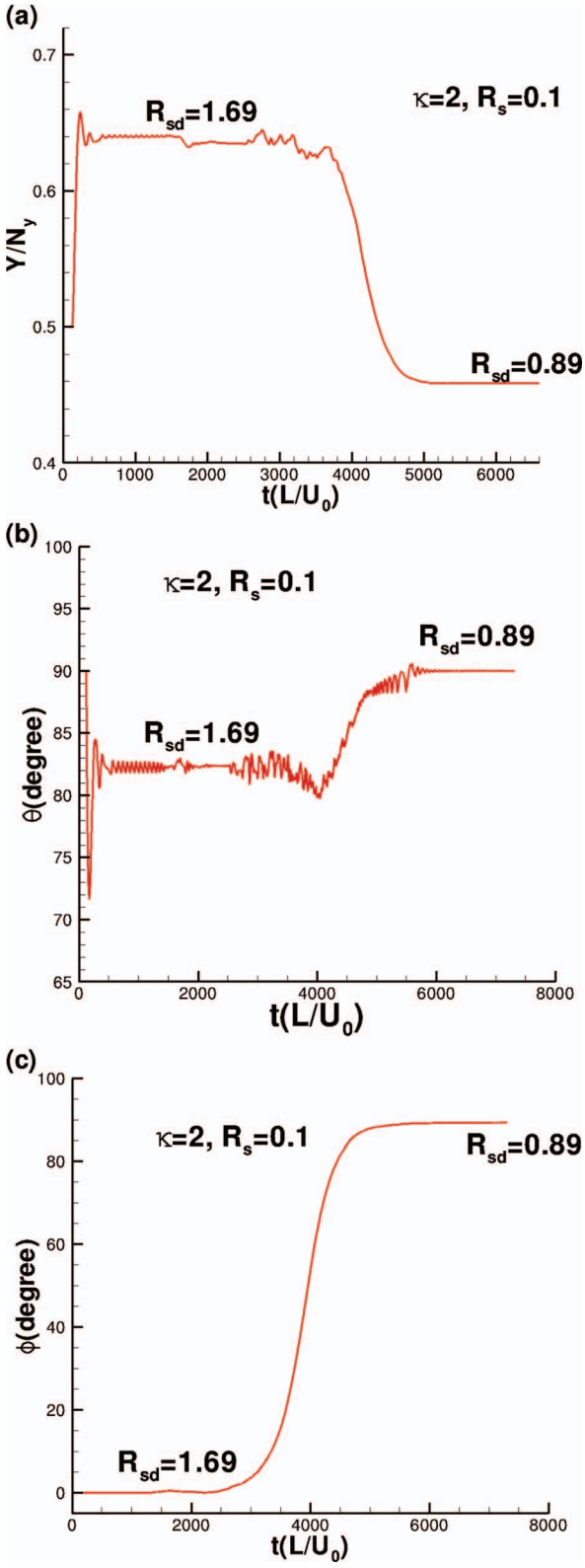

FIG. 10. (a) The fiber lateral migration, (b) orientational angle θ, and (c) plane rotational angle ϕ at $R_s = 0.1$ for the case of $\kappa = 2$. In the short run, the fiber migrates in phase 2 with a settling Reynolds number of $R_{sd} = 1.69$. After a long run, the fiber plane rotational angle becomes $\phi = 90^\circ$, its long axis is along the vorticity direction, thus the fiber migrates and settles with $R_{sd} = 0.89$ in phase 1.

ACKNOWLEDGMENTS

We are grateful to Dr. Don Koch for bringing our attention to this topic. Many valuable ideas and suggestions from him and Dr. Ganesh Subramanian have been used in this work. The use of the computer cluster in the Center for Advanced Vehicle Design and Simulation, Western Michigan University, is also acknowledged.

[1] D. L. Koch and E. S. G. Shaqfeh, "The instability of a dispersion of sedimenting spheroid," J. Fluid Mech. **209**, 521–542 (1989).
[2] A. Dahlkild, "Finite wavelength selection for the linear instability of a suspension of settling spheroids," J. Fluid Mech. **689**, 183–202 (2011).
[3] F. Zhang, A. A. Dahlkild, and F. Lundell, "Nonlinear disturbance growth during sedimentation in dilute fibre suspensions," J. Fluid Mech. **719**, 268–294 (2013).
[4] É. Guazzelli and E. J. Hinch, "Fluctuations and instability in sedimentation," Annu. Rev. Fluid Mech. **43**, 97–116 (2011).
[5] M. B. Mackaplow and E. S. G. Shaqfeh, "A numerical study of the sedimentation of fibre suspensions," J. Fluid Mech. **376**, 149 (1998).
[6] B. Herzhaft and É. Guazzelli, "Experimental study of the sedimentation of dilute and semi-dilute suspensions of fibres," J. Fluid Mech. **384**, 133 (1999).
[7] D. Saintillan, E. Darve, and E. S. G. Shaqfeh, "A smooth particle-mesh Ewald algorithm for Stokes suspension simulations: The sedimentation of fibers," Phys. Fluids **17**, 033301 (2005).
[8] B. Herzhaft, É. Guazzelli, M. Mackaplow, and E. S. G. Shaqfeh, "An experimental investigation of the sedimentation of a dilute fiber suspension," Phys. Rev. Lett. **77**, 290–293 (1996).
[9] J. E. Butler and E. S. G. Shaqfeh, "Dynamic simulations of the inhomogenous sedimentation of rigid fibers," J. Fluid Mech. **468**, 205–237 (2002).
[10] D. Saintillan, E. S. G. Shaqfeh, and E. Darve, "The growth of concentration fluctuations in diluted suspensions of orientable and deformable particles under sedimentation," J. Fluid Mech. **553**, 347–388 (2006).
[11] R. E. Khayat and R. G. Cox, "Inertia effects on the motion of long slender bodies," J. Fluid Mech. **209**, 435 (1989).
[12] M. Shin, D. L. Koch, and G. Subramanian, "A pseudo-spectral method to evaluate the fluid velocity produced by an array of translating slender fibers," Phys. Fluids **18**, 063301 (2006).
[13] M. Shin, D. L. Koch, and G. Subramanian, "Structure and dynamics of dilute suspensions of finite Reynolds number settling fibers," Phys. Fluids **21**, 123304 (2009).
[14] P. G. Saffman, "The lift force on a small sphere in a slow shear flow," J. Fluid Mech. **22**, 385 (1965).
[15] J. B. McLaughlin, "Inertial migration of a small sphere in a linear shear flow," J. Fluid Mech. **224**, 261 (1991).
[16] C. J. Lawrence and R. Mei, "Long-time behaviour of the drag on a body in impulsive motion," J. Fluid Mech. **283**, 307–327 (1995).
[17] R. Mei, "An approximate expression for the shear lift force on a spherical particle at finite Reynolds number," Int. J. Multiphase Flow **18**, 145 (1992).
[18] D. S. Dandy and H. A. Dwyer, "A sphere in shear flow at finite Reynolds number: Effect of shear on particle lift, drag, and heat transfer," J. Fluid Mech. **216**, 381 (1990).
[19] P. Bagchi and S. Balachandar, "Effect of free rotation on the motion of a solid sphere in linear shear flow at moderate Re," Phys. Fluids **14**, 2719 (2002).
[20] E. Kuusela, K. Hofler, and S. Schwarzer, "Computation of particle settling speed and orientation distribution in suspensions of prolate spheroid," J. Eng. Math. **41**, 221–235 (2001).
[21] E. Kuusela, J. M. Lahtinen, and T. Ala-Nissila, "Collective effects in settling of spheroid under steady-state sedimentation," Phys. Rev. Lett. **90**, 094502 (2003).
[22] G. B. Jeffrey, "The motion of ellipsoidal particles immersed in a viscous fluid," Proc. R. Soc. London, Ser. A **102**, 161 (1922).
[23] X. Shan, X. Yuan, and H. Chen, "Kinetic theory representation of hydrodynamics: A way beyond the Navier-Stokes equation," J. Fluid Mech. **550**, 413–441 (2006).
[24] A. J. C. Ladd, "Numerical simulations of particle suspensions via a discretised Boltzmann equation. Part 1. Theoretical foundation," J. Fluid Mech. **271**, 285 (1994).
[25] C. K. Aidun, Y. Lu, and E. Ding, "Direct analysis of particulate suspensions with inertia using the discrete Boltzmann equation," J. Fluid Mech. **373**, 287 (1998).
[26] D. Qi, "Lattice Boltzmann simulations of particles in non-zero Reynolds number flows," J. Fluid Mech. **385**, 41 (1999).
[27] D. Qi, "Direct simulations of flexible cylindrical fiber suspensions in finite Reynolds number flows," J. Chem. Phys. **125**, 114901 (2006).
[28] D. L. Koch and A. J. C. Ladd, "Moderate Reynolds number flows through periodic and random arrays of aligned cylinders," J. Fluid Mech. **349**, 31 (1997).
[29] D. Qi and L.-S. Luo, "Rotational and orientational behavior of spheroidal particles in a Couette flows," J. Fluid Mech. **477**, 201–213 (2003).
[30] G. Segré and A. Silberbergi, "Radial Poiseuille flows of suspensions," Nature (London) **189**, 209 (1961).
[31] G. Segré and A. Silberbergi, "Behavior of macroscopic rigid spheres in Poiseuille flow Part 1. Determination of local concentration by statistical analysis of particle passages through crossed light beams," J. Fluid Mech. **14**, 115 (1962).
[32] D. Qi, L. S. Luo, R. Aravamuthan, and W. Streider, "Lateral migration and orientation of elliptical particles in Poiseuille flows," J. Stat. Phys. **107**, 101–120 (2002).
[33] P. Y. Huang, J. Fang, and D. Joseph, "The turning couples on an elliptic particle settling in a vertical channel," J. Fluid Mech. **271**, 1–16 (1994).